

Uncovering the Metabolic Origin of Aspartate for Tumor Growth Using an Integrated Molecular Deactivator

Ruixue Duan,[◆] Yuanyuan Xu,[◆] Xuemei Zeng, Jiahui Xu, Liangliang Liang, Zhenzhen Zhang, Zhimin Wang, Xiaoxiao Jiang, Bengang Xing, Bifeng Liu, Angelo All, Xiaosong Li,^{*} Luke P. Lee,^{*} and Xiaogang Liu^{*}



Cite This: <https://dx.doi.org/10.1021/acs.nanolett.0c04520>



Read Online

ACCESS |



Metrics & More



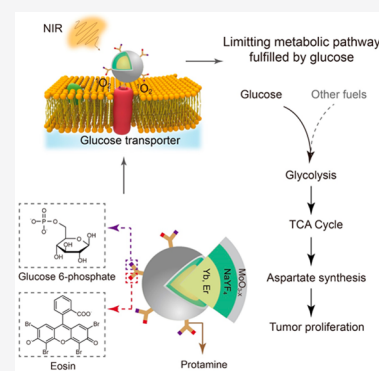
Article Recommendations



Supporting Information

ABSTRACT: Reprogrammed glucose metabolism is vital for cancer cells, but aspartate, an intermediate metabolic product, is the limiting factor for cancer cell proliferation. However, due to the complexity of metabolic pathways, it remains unclear whether glucose is the primary source of endogenous aspartate. Here, we report the design of an innovative molecular deactivator, based on a multifunctional upconversion nanoprobe, to explore the link between glucose and aspartate. This molecular deactivator mainly works in the acidic, hypoxic tumor microenvironment and deactivates multiple types of glucose transporters on cancer cell membranes upon illumination at 980 nm. Cancer cell proliferation *in vivo* is strongly inhibited by blocking glucose transporters. Our experimental data confirm that the cellular synthesis of aspartate for tumor growth is glucose-dependent. This work also demonstrates the untapped potential of molecularly engineered upconversion nanoprobe for discovering hidden metabolic pathways and improving therapeutic efficacy of conventional antitumor drugs.

KEYWORDS: *Upconversion nanoprobe, protein deactivation, glucose transporter, cell metabolism, glucose-derived aspartate*



INTRODUCTION

Rewired glucose metabolism with increased glucose utilization is a hallmark of cancer.^{1–5} Altered glucose metabolism generates energy and precursor metabolites related to the synthesis of nucleic acids, lipids, and proteins. Although various studies have investigated glucose metabolism in relation to malignancy using *in vitro* cell culture models,^{6,7} the metabolic behavior of cancer cells *in vitro* is quite different from that *in vivo* in the complex tumor microenvironment.^{8,9} Isotope-tracer-assisted methods have been used to study reprogrammed glucose metabolic flux in tumors,^{3,10,11} but due to metabolic compensation, these methods yield more information about the state of glucose and its metabolites than about the impact of glucose on the downstream network.¹² Developing methods that block glucose uptake in tumor cells is critical to understand fundamental mechanisms by which glucose sustains tumor growth.¹³ As aspartate, synthesized by cells, is a limiting metabolite for tumor growth,^{3,4} determining whether glucose is an essential source of intracellular aspartate may prove efficacious in cancer treatment. Various inhibitory small molecules and antibodies target cell-membrane glucose transporters.^{14,15} However, these inhibitors lack the capacity to block multiple types of glucose transporters, with the result that they cannot prevent glucose uptake by cancer cells. Another challenge in targeting glucose transporters *in vivo* is the high likelihood of nonselective cytotoxicity for surrounding healthy cells.

Inspired by recent developments in molecular engineered nanomaterials for cancer diagnostics and therapeutics,^{16–21} we decided to probe the link between glucose and aspartate by designing an integrated molecular deactivator (iMD). This general concept involves a lanthanide-doped upconversion nanoparticle core with a thin layer of reduced molybdenum oxide (MoO_{3-x}) nanosheets modified with glucose phosphate, eosin, and protamine (Figure 1a). This nanoscale iMD is stable in the acidic, hypoxic tumor microenvironment, and it selectively binds to tumor tissue. Moreover, iMD nanoprobe (iMDs) disassemble under normal physiological conditions due to degradation of MoO_{3-x} nanosheets into ultrasmall nanoparticles. The MoO_{3-x} nanosheets provide a link between phosphate glucose/photosensitizers and upconversion nanoparticles, while protecting the nanoprobe from damage by adjacent normal cells. Glucose phosphate on the iMDs enables diverse glucose transporter isoforms to be recognized on cancer cell membranes due to the interaction of glucose and glucose transporters. When illuminated at 980 nm, iMDs generate singlet oxygen species from the photosensitizer, eosin. As the

Received: November 16, 2020

Revised: December 3, 2020

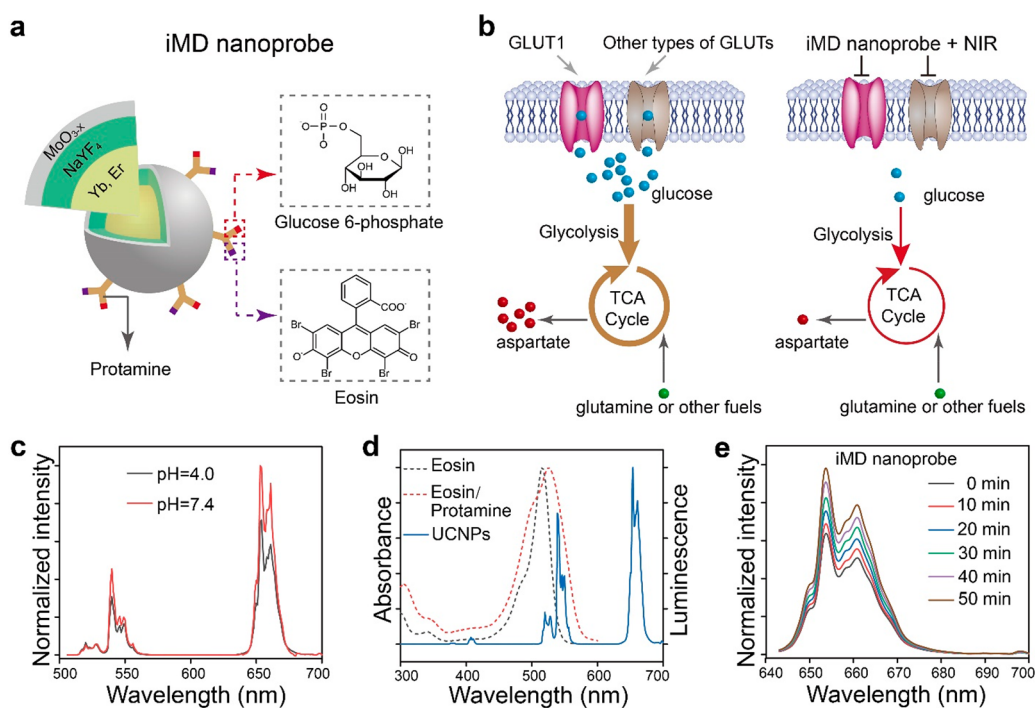


Figure 1. iMDs deactivate multiple types of glucose transporters on cancer cell membranes, blocking glucose uptake and curtailing aspartate production. (a) Schematic design of an iMD comprising a core-shell upconversion nanoparticle, with a thin layer of MoO_{3-x} for targeting the tumor microenvironment, eosin photosensitizer, glucose phosphate to target glucose transporters, and protamine to stabilize MoO_{3-x} and to link eosin and glucose phosphate. (b) Schematic depicting the proposed processes of glucose metabolism in the absence (left) and presence (right) of iMDs. Tumor growth relies on glycolysis through glucose uptake but is limited by aspartate synthesized via the TCA cycle. In the presence of iMDs and NIR illumination, glucose transporters are deactivated, leading to inhibition of glucose uptake, glycolysis, the TCA cycle, and aspartate synthesis. Importantly, other fuel substrates for cultured cancer cells, such as glutamine, do not support the TCA cycle by acting as substitutes for glucose *in vivo*. TCA, tricarboxylic acid; GLUT1, glucose transporter 1; GLUTs, glucose transporters. (c) Photoluminescence emission spectra of the iMDs dispersed in two aqueous solutions (pH 4.0 and 7.4). An increase in emission intensity of iMDs at 660 nm suggests degradation of the MoO_{3-x} coating at pH 7.4. (d) Absorption spectra recorded for eosin and a mixture of eosin and protamine and the photoluminescence emission spectrum of $\text{NaYF}_4:\text{Yb}/\text{Er}@ \text{NaYF}_4$ nanoparticles. (e) Time-dependent measurements of singlet oxygen production assessed based on NIR illumination of iMDs dispersed in pH 4.0 aqueous solution. Increased emission intensity indicates degradation of the MoO_{3-x} coating in the presence of singlet oxygen.

half-radius range of damage by singlet oxygen species is about 3–4 nm (ref 22), only glucose transporters interacting with iMDs will be deactivated with high spatial and temporal resolutions, avoiding unintended oxidation of other proteins on cancer cell membranes. Unlike traditional inhibitors of glucose transporters, our iMDs deactivate various types of glucose transporters, thereby blocking glucose transport across the plasma membrane (Figure 1b). Glucose deprivation inhibits glycolysis and the tricarboxylic acid (TCA) cycle, impairing energy generation and aspartate production in cancer cells. Notably, glutamine or other fuel substrates utilized by cultured cancer cells does not act as an alternative energy substrate to rescue the suppressed TCA cycle in HeLa xenograft mouse models.^{7,8}

RESULTS

Preparation of iMDs. To form functional iMDs, $\text{NaYF}_4:\text{Yb}/\text{Er}@ \text{NaYF}_4$ nanoparticles, which are capable of converting near-infrared (NIR) light into visible emission,^{23–27} were synthesized and coated with a thin layer of pH-responsive MoO_{3-x} (Figure S1). Subsequently, eosin photosensitizer and glucose phosphate were coated onto nanoparticle surfaces using protamine, an alkaline protein, as the linker (Figure S2). Characterizations of iMDs were established by dynamic light scattering measurements and Fourier transform infrared spectroscopy (Figure S3). Degradation of the MoO_{3-x} coating under

physiological conditions (pH 7.4) was confirmed by monitoring the emission intensity of iMDs at 660 nm with 980 nm excitation (Figure 1c).

We next confirmed the capacity of nanoscale iMDs to produce singlet oxygen species under NIR excitation, which was facilitated by spectral overlap between green emission at 545 nm from $\text{NaYF}_4:\text{Yb}/\text{Er}@ \text{NaYF}_4$ nanoparticles and absorption of the eosin photosensitizer tethered on nanoparticle surfaces (Figure 1d). We observed a decline in emission intensity of iMDs with an increasing concentration of surface-tethered eosin (Figure S4). Given that MoO_{3-x} could also be oxidized and slowly degraded in the presence of singlet oxygen,²⁸ generation of singlet oxygen species from iMDs was monitored using time-dependent upconversion photoluminescence (Figure S4). Under 980 nm illumination, iMDs generated singlet oxygen and caused MoO_{3-x} degradation, as evidenced by the gradual recovery in emission intensity at 660 nm (Figure 1e).

iMD Probe Inhibits Glucose Uptake and Induces Cell Apoptosis at the Cellular Level. We introduced fluorescent glucose analogues to monitor glucose transporter activity at the cellular level in iMD-treated HeLa cells. Our analysis revealed that, without NIR exposure, glucose uptake by cancer cells was suppressed within 30 min of incubation with fluorescent glucose analogues and then recovered after 4 h (Figure 2a). In contrast, with NIR treatment, we observed reduced glucose uptake even after 4 h. Our results suggest that, with NIR illumination, cancer

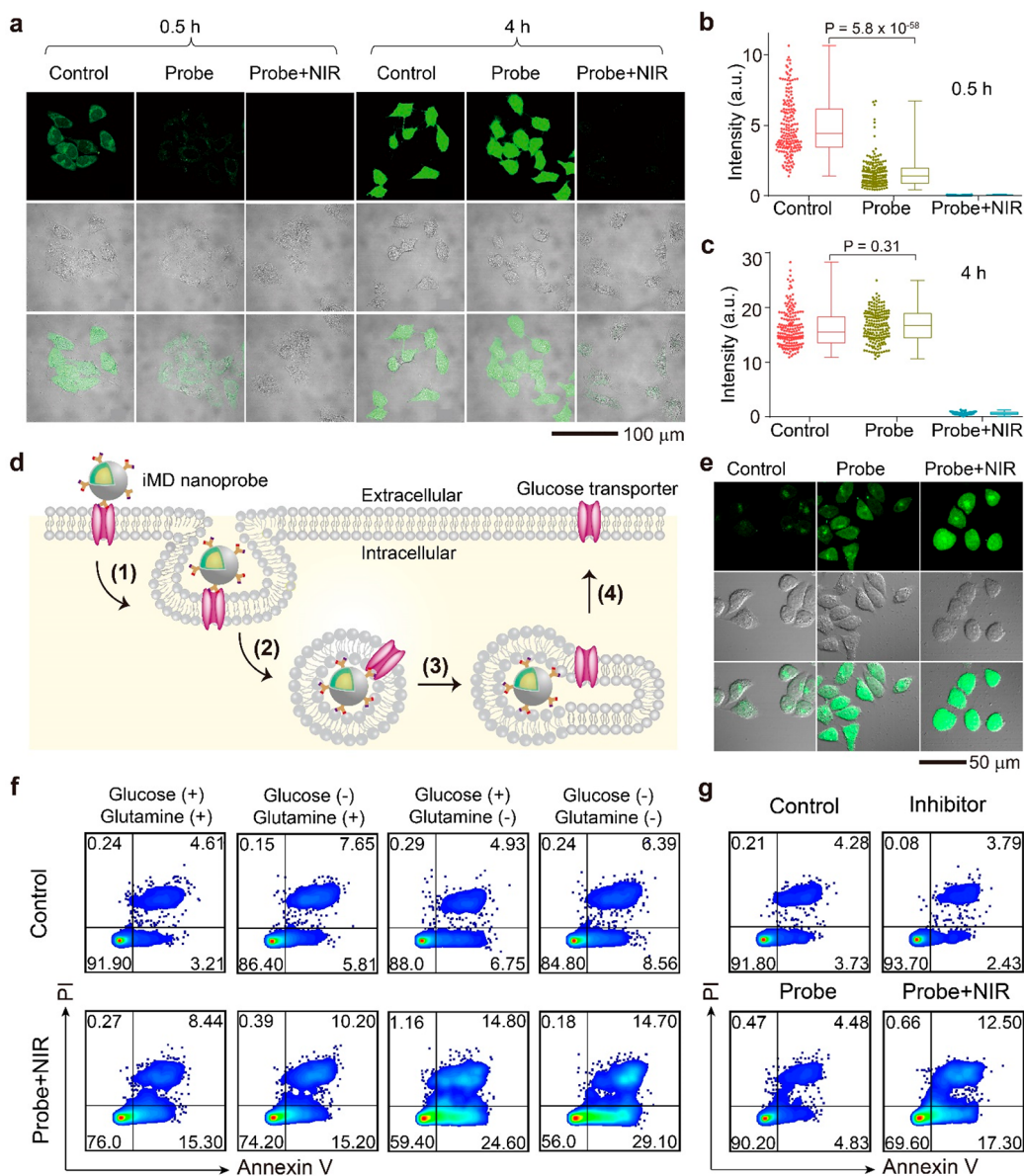


Figure 2. iMDs inhibit glucose uptake and elicit cell apoptosis. (a) Fluorescence images of 2-NBDG-stained cancer cells upon photon upconversion treatment, recorded after dye incubation for 30 min and 4 h. Note that the fluorescence of iMD-treated cells without NIR illumination recovers after 4 h of dye incubation. In contrast, under NIR illumination, fluorescence of iMD-treated cells is completely quenched. (b,c) Statistical analyses of imaging data, obtained after 2-NBDG dye incubation for 30 min and 4 h, respectively. A two-tailed Student's *t* test was employed. (d) Proposed mechanism of temporary fluorescence quenching over iMD-treated cells in the absence of laser illumination. Upon incubation with cells, nanoprobe is internalized via endocytosis (step 1), followed by endocytic vesicle formation (step 2) and endosomal sorting (step 3). Glucose transporters are then recycled back to the plasma membrane, making them available for 2-NBDG dye staining (step 4). (e) Intracellular calcium signaling validation of glucose deprivation of cells treated with either iMDs alone or in combination with NIR light illumination. (f) Effects of various cell culture media on untreated or iMD-treated cancer cells. (g) Flow cytometry analyses of untreated cells and cells exposed to commercial WZB117 inhibitor and iMDs in the absence and presence of NIR light illumination, respectively. A significant level of cell apoptosis only occurs under photon upconversion conditions.

cells essentially lost glucose transport capacity (Figure 2b,c). This phenomenon was also observed in a HepG2 cell line (Figure S5). We reasoned that, without NIR illumination, interaction of the iMD with glucose transporters is likely to induce internalization of glucose transporters, leading to a decrease in glucose uptake. Notably, glucose uptake can recover after glucose transporters recycle back to the cell membrane (Figure 2d) (ref 29). In addition, inhibition of glucose uptake by the iMD was further confirmed by observation of increased intracellular calcium signaling with or without NIR illumination (Figure 2e). The effect of cell culture medium on iMD treatment

was also investigated (Figure 2f). Results of flow cytometry analysis showed that glucose uptake was inhibited in treated cancer cells, as evidenced by the change in apoptosis levels in the culture medium in the presence or absence of glucose. Intriguingly, results from control groups suggested that there were multiple routes to provide a carbon source for cultured cancer cell growth. It also should be noted that, after incubation for an additional 12 h, treated cancer cells showed low levels of necrosis, indicating that treatment was promoted by a glucose transporter rather than through a whole cell membrane. Furthermore, flow cytometry analysis of HeLa cells, upon

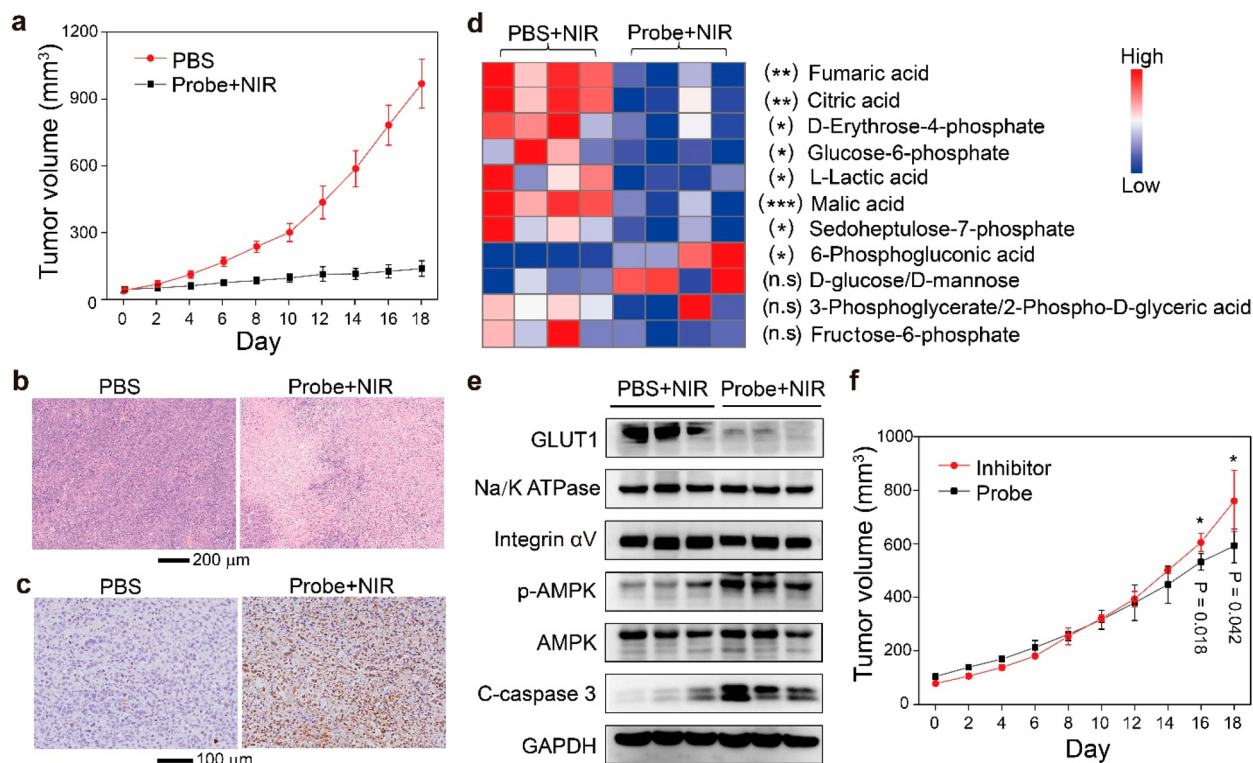


Figure 3. iMDs improve antitumor efficiency in vivo by inhibiting glucose metabolism. (a) Tumor growth curves obtained after treatment with either phosphate-buffered saline or iMDs plus NIR illumination. $N = 6$ mice/group (error bars show mean \pm SD). (b) H&E histology of tumor sections for tumors treated with either phosphate-buffered saline or iMDs plus NIR light illumination. (c) Immunohistochemical data obtained with immunostaining for cleaved caspase-3 (brown color) with different treatments. (d) Heatmap of LC-MS data showing tumor metabolite changes after nanoprobe treatment with 980 nm illumination. Increases in metabolite levels are shown in red, whereas blue indicates decreased metabolite titers. A two-tailed Student's t test was employed for statistical analysis. (e) Immunoblots of GLUT1, Na-K-ATPase, and integrin α V in the tumors treated with either phosphate-buffered saline plus 980 nm illumination or iMDs plus NIR light illumination. (f) Tumor growth curves recorded after treatment with the GLUT1 pharmacological inhibitor, WZB117, or iMDs without 980 nm illumination. $N = 4$ mice/group. A two-tailed Student's t test was employed for statistical analysis.

upconversion activation, showed an about 3.72-fold increase in apoptosis compared to cells incubated with WZB117 inhibitor or iMDs alone (Figure 2g).

iMD Probe Suppresses Tumor Growth by Blocking Glucose Metabolism. We next investigated whether our strategy inhibits tumor growth in vivo. Tumor-bearing mice were treated with an intratumor injection of iMDs, followed by 980 nm illumination. Our results showed that this approach inhibited tumor growth (Figure 3a). To assess the antitumor therapeutic efficacy of iMDs, we further performed a histological examination of tumor tissue after 18 days of iMD treatment. Significant necrosis was observed for tumors treated with 980 nm laser-induced photodynamic therapy compared to that with untreated controls (Figure 3b). Consistent with reduced tumor volume and H&E staining, immunohistochemical analysis of tissues upon photon upconversion-based treatment revealed a high-level expression of cleaved caspase-3, an apoptosis marker (Figure 3c). It is noteworthy that, with the influence of NIR light, NaYF₄:Yb/Er@NaYF₄ and MoO_{3-x} on tumor growth can be ruled out based on experimental data from another control group in which mouse tumors were injected with NaYF₄:Yb/Er@NaYF₄@MoO_{3-x} nanoparticles (Figure S6). We also injected iMDs into mice intravenously and evaluated their biocompatibility and safety. Routine blood analysis and histological H&E staining on day 18 and day 80 after intravenous injection showed statistically no significant differ-

ence between untreated controls and treated mice (Figures S7 and S8).

To investigate the mechanism by which deactivated glucose transporters selectively inhibit tumor development, we used mass spectrometry to examine metabolomic changes of HeLa xenografts after optical manipulation of iMDs (Figure 3d). Targeted metabolism analysis confirmed that optical manipulation of iMDs inhibited relative metabolite levels of glycolysis, the pentose phosphate pathway, and the TCA cycle (Figure S9). Tumor cell apoptosis and energy stress were evident from increased concentrations of cleaved caspase-3 or p-AMPK proteins, respectively (Figure 3e). The high specificity of our iMDs for targeting glucose transporters was confirmed by analyzing expression of three types of membrane proteins after the treatment of iMDs. Interestingly, consistent with cellular experiments carried out without NIR illumination, iMDs in vivo were more effective than the WZB117 inhibitor in suppressing tumor growth (Figure 3f).

Transformation from Glucose to Aspartate Is the Limiting Metabolic Pathway for Tumor Growth. Recent evidence shows that most tumors rely heavily on glucose for proliferation, and aspartate is a critical product of mitochondrial respiration.³⁰⁻³² Therefore, we hypothesize that deactivation of glucose transporters might inhibit aspartate production. To confirm therapeutic mechanisms, we further evaluated 457 metabolites by implementing an untargeted metabolomic method (Supporting Information) and found that 129

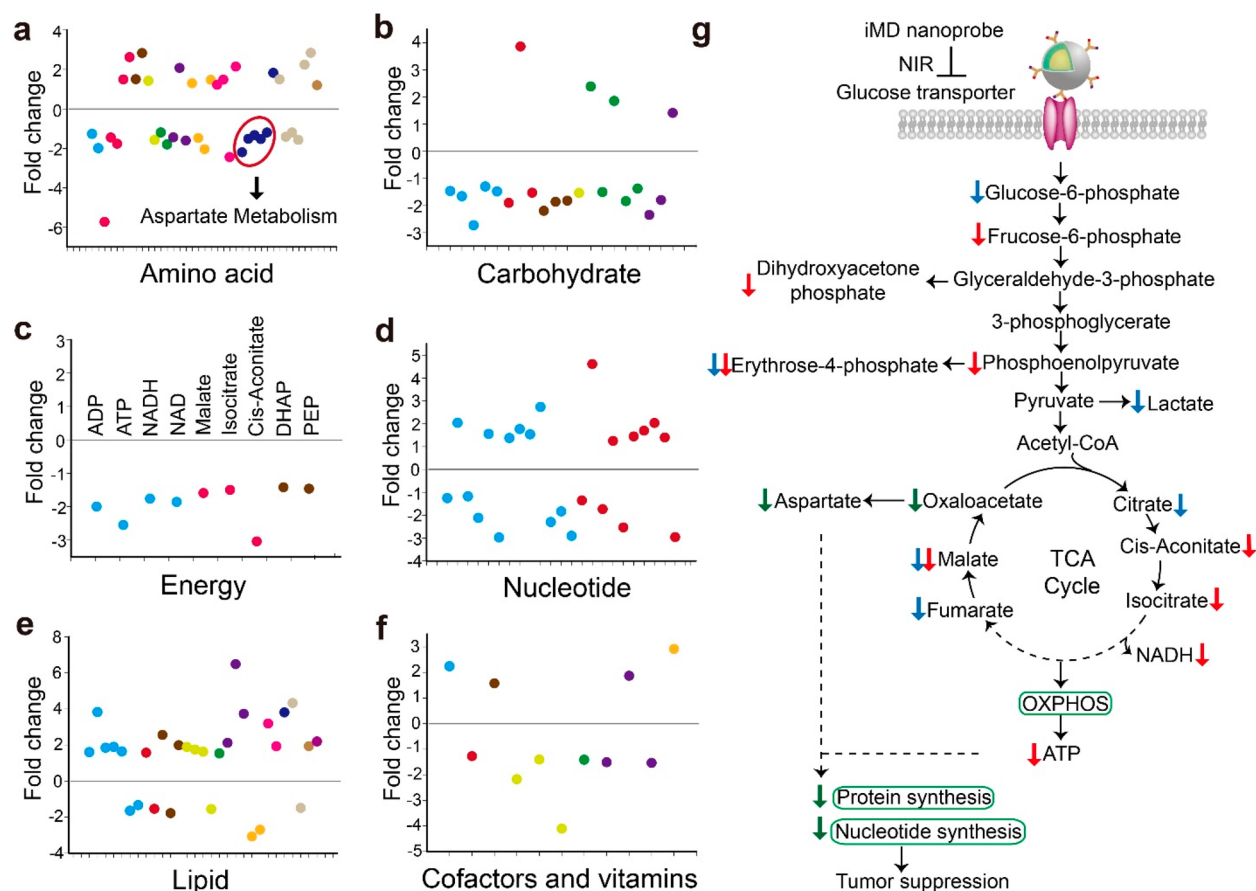


Figure 4. iMDs confirm that aspartate, essential to tumor growth, depends upon glucose transport and metabolism. (a–f) Effects of iMDs on amino acid, carbohydrate, energy, nucleotide, lipid, and cofactor metabolism. Negative or positive changes (fold) indicate down-regulated or up-regulated metabolite levels in treated groups compared to the control group, respectively. Dot colors represent metabolic pathways to which different metabolites pertain (Supporting Information) and affected significantly (Student's *t* test, $p < 0.05$) in treated groups. Blue dots inside the red circle (a) indicate metabolites associated with aspartate metabolism (Supporting Information Figure 11). Treated groups: tumor xenografts were injected with iMDs, followed by NIR light illumination. Control group: tumor xenografts were injected with phosphate-buffered saline, followed by NIR light illumination. $N = 5$ mice/group. ADP, adenosine 5'-diphosphate; ATP, adenosine 5'-triphosphate; NADH, reduced nicotinamide adenine dinucleotide; NAD, nicotinamide adenine dinucleotide; DHAP, dihydroxyacetone phosphate; PEP, phosphoenolpyruvate. (g) Schematic showing how iMDs block respiration and suppress tumor growth under NIR light illumination. Blue and red arrows indicate metabolites identified by targeted and untargeted metabolomic experiments, respectively. Green arrows denote possible suppression of metabolites and pathways that are likely involved in tumor suppression.

metabolites were strongly reduced by the treatment (Student's *t* test, $p < 0.05$). Affected metabolites pertain to six metabolic pathways, each linked to glucose metabolism (Figure 4a–f, and Supporting Information Figure S10). This untargeted metabolomic profiling also showed that depletion of mitochondrial substrates due to glycolytic inhibition contributes to energy stress and aspartate deficiency in xenografts (Figure S11). In summary, deactivation of glucose transporters by iMDs blocks glycolysis and the TCA cycle, indicating that neither glutamine metabolism nor alternative pathways compensated for glucose metabolism (Figure 4g). This limits generation of ATP and aspartate and ultimately suppresses tumor growth.

DISCUSSION

Molecular inhibitors have been widely used therapeutically to inhibit cancer cell proliferation. Nevertheless, the clinical efficacy of these molecules has been confounded by many factors, particularly the lack of a robust and quantitative technique for screening target-specific inhibitors. Here, we have introduced an iMD that inhibits tumor growth by targeting multiple types of glucose transporters. The value of this

translational approach is that nonselective cytotoxicity of conventional molecular inhibitors is mitigated. Suppression of the TCA cycle suggests that production of aspartate is directly governed by glucose in tumor development. Our findings illustrate the great potential of integrating functional molecules and optical nanomaterials as not only fundamental discovery devices but also therapeutic tools.

ASSOCIATED CONTENT

Supporting Information

The Supporting Information is available free of charge at <https://pubs.acs.org/doi/10.1021/acs.nanolett.0c04520>.

Detailed experimental methods; characterization of MoO_{3-x} ; demonstration of the function of the iMD probe; evaluations of the iMD probe at the cellular level and in vivo; biosafety evaluation data; targeted and untargeted metabolomic analysis; aspartate metabolism analysis, uncropped raw data of Western blots; photographs of tumor-bearing mice after different treatments (PDF)

■ AUTHOR INFORMATION

Corresponding Authors

Xiaosong Li – Department of Oncology, The Fourth Medical Center of Chinese People's Liberation Army General Hospital, Beijing 100048, China; Jinzhou Medical University, Jinzhou 121001, China; Email: lixiaosong@301hospital.com.cn

Luke P. Lee – Berkeley Sensor and Actuator Centre, Department of Bioengineering, Department of Electrical Engineering and Computer Science, and Biophysics Graduate Program, University of California at Berkeley, Berkeley, California 94720, United States; Department of Medicine, Harvard Medical School, Brigham and Women Hospital, Boston, Massachusetts 02115, United States; Biomedical Institute of Global Healthcare Research and Technology (BIGHEART), National University of Singapore, Singapore 117456; orcid.org/0000-0002-1436-4054; Email: lplee@bwh.harvard.edu

Xiaogang Liu – Department of Chemistry, Biomedical Institute of Global Healthcare Research and Technology (BIGHEART), and The N.1 Institute for Health, National University of Singapore, Singapore 117543; orcid.org/0000-0003-2517-5790; Email: chmlx@nus.edu.sg

Authors

Ruixue Duan – Department of Chemistry, National University of Singapore, Singapore 117543

Yuanyuan Xu – Department of Oncology, The Fourth Medical Center of Chinese People's Liberation Army General Hospital, Beijing 100048, China; Jinzhou Medical University, Jinzhou 121001, China

Xuemei Zeng – Department of Biomedical Engineering, College of Life Science and Technology, Huazhong University of Science and Technology, Wuhan 430074, China

Jiahui Xu – Department of Chemistry, National University of Singapore, Singapore 117543

Liangliang Liang – Department of Chemistry, National University of Singapore, Singapore 117543; orcid.org/0000-0003-4958-3801

Zhenzhen Zhang – Institute for Brain Research and Rehabilitation, South China Normal University, Guangzhou 510631, China

Zhimin Wang – Division of Chemistry and Biological Chemistry, School of Physical & Mathematical Sciences, Nanyang Technological University, Singapore 637371

Xiaoxiao Jiang – Key Laboratory of Animal Ecology and Conservation Biology, Institute of Zoology, Chinese Academy of Sciences, Beijing 100101, China

Bengang Xing – Division of Chemistry and Biological Chemistry, School of Physical & Mathematical Sciences, Nanyang Technological University, Singapore 637371; orcid.org/0000-0002-8391-1234

Bifeng Liu – Department of Biomedical Engineering, College of Life Science and Technology, Huazhong University of Science and Technology, Wuhan 430074, China

Angelo All – Department of Chemistry, Hong Kong Baptist University, Kowloon Tong, Hong Kong SAR, China

Complete contact information is available at:

<https://pubs.acs.org/10.1021/acs.nanolett.0c04520>

Author Contributions

• R.D. and Y.X. contributed equally to this work.

Notes

The authors declare no competing financial interest.

■ ACKNOWLEDGMENTS

This work was supported by the Singapore Ministry of Education (MOE2017-T2-2-110), the Agency for Science, Technology and Research (A*STAR) (Grant No. A1883c0011), the National Research Foundation, the Prime Minister's Office of Singapore under its Competitive Research Program (Award No. NRF-CRP15-2015-03). Support was also provided by the NRF Investigatorship programme (Award No. NRF-NRFI05-2019-0003), NUS NANONASH Programme (NUHSRO/2020/002/NanoNash/LOA; R143000B43114), the National Natural Science Foundation of China (21771135 and 81572953), and the National Key Research and Development Program of China (2018YFB0407200). We thank Q. Wei, S. Yan, Y. He, X. Liu, and Y. Wu for helpful discussion and experimental assistance.

■ REFERENCES

- (1) DeBerardinis, R. J.; Chandel, N. S. Fundamentals of cancer metabolism. *Sci. Adv.* **2016**, *2*, No. e1600200.
- (2) Hay, N. Reprogramming glucose metabolism in cancer: can it be exploited for cancer therapy? *Nat. Rev. Cancer* **2016**, *16*, 635–649.
- (3) Sullivan, L. B.; Luengo, A.; Danai, L. V.; Bush, L. N.; Diehl, F. F.; Hosios, A. M.; Lau, A. N.; Elmiligy, S.; Malstrom, S.; Lewis, C. A.; Vander Heiden, M. G. Aspartate is an endogenous metabolic limitation for tumour growth. *Nat. Cell Biol.* **2018**, *20*, 782–788.
- (4) Garcia-Bermudez, J.; Baudrier, L.; La, K.; Zhu, X. G.; Fidelin, J.; Sviderskiy, V. O.; Papagiannakopoulos, T.; Molina, H.; Snuderl, M.; Lewis, C. A.; Possemato, R. L.; Birsoy, K. Aspartate is a limiting metabolite for cancer cell proliferation under hypoxia and in tumours. *Nat. Cell Biol.* **2018**, *20*, 775–781.
- (5) Hensley, C. T.; Faubert, B.; Yuan, Q.; Lev-Cohain, N.; Jin, E.; Kim, J.; Jiang, L.; Ko, B.; Skelton, R.; Loudat, L.; Wodzak, M.; Klimko, C.; McMillan, E.; Butt, Y.; Ni, M.; Oliver, D.; Torrealba, J.; Malloy, C. R.; Kernstine, K.; Lenkinski, R. E.; DeBerardinis, R. J. Metabolic Heterogeneity in Human Lung Tumors. *Cell* **2016**, *164*, 681–694.
- (6) Lee, H. Y.; Itahana, Y.; Schuechner, S.; Fukuda, M.; Je, H. S.; Ogris, E.; Virshup, D. M.; Itahana, K. Ca²⁺-dependent demethylation of phosphatase PP2Ac promotes glucose deprivation-induced cell death independently of inhibiting glycolysis. *Sci. Signaling* **2018**, *11*, No. eaam7893.
- (7) Birsoy, K.; Possemato, R.; Lorbeer, F. K.; Bayraktar, E. C.; Thiru, P.; Yucel, B.; Wang, T.; Chen, W. W.; Clish, C. B.; Sabatini, D. M. Metabolic determinants of cancer cell sensitivity to glucose limitation and biguanides. *Nature* **2014**, *508*, 108–112.
- (8) Muir, A.; Vander Heiden, M. G. The nutrient environment affects therapy. *Science* **2018**, *360*, 962–963.
- (9) Yi, W.; Clark, P. M.; Mason, D. E.; Keenan, M. C.; Hill, C.; Goddard, W. A., III; Peters, E. C.; Driggers, E. M.; Hsieh-Wilson, L. C. Phosphofructokinase 1 glycosylation regulates cell growth and metabolism. *Science* **2012**, *337*, 975–980.
- (10) Vincent, E. E.; Sergushichev, A.; Griss, T.; Gingras, M.-C.; Samborska, B.; Ntimbane, T.; Coelho, P. P.; Blagih, J.; Raissi, T. C.; Choiniere, L.; Bridon, G.; Loginicheva, E.; Flynn, B. R.; Thomas, E. C.; Tavare, J. M.; Avizonis, D.; Pause, A.; Elder, D. J.E.; Artyomov, M. N.; Jones, R. G. Mitochondrial Phosphoenolpyruvate Carboxykinase Regulates Metabolic Adaptation and Enables Glucose-Independent Tumor Growth. *Mol. Cell* **2015**, *60*, 195–207.
- (11) Courtney, K. D.; Bezwada, D.; Mashimo, T.; Pichumani, K.; Vemireddy, V.; Funk, A. M.; Wimberly, J.; McNeil, S. S.; Kapur, P.; Lotan, Y.; Margulis, V.; Cadeddu, J. A.; Pedrosa, I.; DeBerardinis, R. J.; Malloy, C. R.; Bachoo, R. M.; Maher, E. A. Isotope tracing of human clear cell renal cell carcinomas demonstrates suppressed glucose oxidation *in vivo*. *Cell Metab.* **2018**, *28*, 793–800.

- (12) Jang, C.; Chen, L.; Rabinowitz, J. D. Metabolomics and isotope tracing. *Cell* **2018**, *173*, 822–837.
- (13) Yun, J.; Rago, C.; Cheong, I.; Pagliarini, R.; Angenendt, P.; Rajagopalan, H.; Schmidt, K.; Willson, J. K. V.; Markowitz, S.; Zhou, S.; Diaz, L. A., Jr; Velculescu, V. E.; Lengauer, C.; Kinzler, K. W.; Vogelstein, B.; Papadopoulos, N. Glucose deprivation contributes to the development of KRAS Pathway mutations in tumor cells. *Science* **2009**, *325*, 1555–1559.
- (14) Chan, D. A.; Sutphin, P. D.; Nguyen, P.; Turcotte, S.; Lai, E. W.; Banh, A.; Reynolds, G. E.; Chi, J.; Wu, J.; Solow-Cordero, D. E.; Bonnet, M.; Flanagan, J. U.; Bouley, D. M.; Graves, E. E.; Denny, W. A.; Hay, M. P.; Giaccia, A. J. Targeting GLUT1 and the Warburg effect in renal cell carcinoma by chemical synthetic lethality. *Sci. Transl. Med.* **2011**, *3*, No. 94ra70.
- (15) Ferguson, F. M.; Gray, N. S. Kinase inhibitors: the road ahead. *Nat. Rev. Drug Discovery* **2018**, *17*, 353–377.
- (16) Cagno, V.; Andreozzi, P.; D'Alicarnasso, M.; Jacob Silva, P.; Mueller, M.; Galloux, M.; Le Goffic, R.; Jones, S. T.; Vallino, M.; Hodek, J.; Weber, J.; Sen, S.; Janecek, E.-R.; Bekdemir, A.; Sanavio, B.; Martinelli, C.; Donalisio, M.; Rameix Welti, M.-A.; Eleouet, J.-F.; Han, Y.; Kaiser, L.; Vukovic, L.; Tapparel, C.; Kral, P.; Krol, S.; Lembo, D.; Stellacci, F. Broad-spectrum non-toxic antiviral nanoparticles with a virucidal inhibition mechanism. *Nat. Mater.* **2018**, *17*, 195–203.
- (17) Chen, S.; Weitemier, A. Z.; Zeng, X.; He, L.; Wang, X.; Tao, Y.; Huang, A. J. Y.; Hashimoto, Y.; Kano, M.; Iwasaki, H.; Parajuli, L. K.; Okabe, S.; Teh, D. B. L.; All, A. H.; Tsutsui-Kimura, I.; Tanaka, K. F.; Liu, X.; McHugh, T. J. Near-infrared deep brain stimulation via upconversion nanoparticle-mediated optogenetics. *Science* **2018**, *359*, 679–684.
- (18) Kam, N. W.; Jan, E.; Kotov, N. A. Electrical stimulation of neural stem cells mediated by humanized carbon nanotube composite made with extracellular matrix protein. *Nano Lett.* **2009**, *9*, 273–278.
- (19) Rosi, N. L.; Rosi, N. L.; Giljohann, D. A.; Thaxton, C. S.; Lytton-Jean, A. K. R.; Han, M. S.; Mirkin, C. A. Oligonucleotide-modified gold nanoparticles for intracellular gene regulation. *Science* **2006**, *312*, 1027–1030.
- (20) Parak, W. J. Controlled interaction of nanoparticles with cells. *Science* **2016**, *351*, 814–815.
- (21) Ohta, S.; Glancy, D.; Chan, W. C. W. DNA-controlled dynamic colloidal nanoparticle systems for mediating cellular interaction. *Science* **2016**, *351*, 841–845.
- (22) Takemoto, K.; Iwanari, H.; Tada, H.; Suyama, K.; Sano, A.; Nagai, T.; Hamakubo, T.; Takahashi, T. Optical inactivation of synaptic AMPA receptors erases fear memory. *Nat. Biotechnol.* **2017**, *35*, 38–47.
- (23) Zhong, Y.; Ma, Z.; Wang, F.; Wang, X.; Yang, Y.; Liu, Y.; Zhao, X.; Li, J.; Du, H.; Zhang, M.; Cui, Q.; Zhu, S.; Sun, Q.; Wan, H.; Tian, Y.; Liu, Q.; Wang, W.; Garcia, K. C.; Dai, H. *In vivo* molecular imaging for immunotherapy using ultra-bright near-infrared-IIb rare-earth nanoparticles. *Nat. Biotechnol.* **2019**, *37*, 1322–1331.
- (24) Zhang, Y.; Zheng, F.; Yang, T.; Zhou, W.; Liu, Y.; Man, N.; Zhang, L.; Jin, N.; Dou, Q.; Zhang, Y.; Li, Z.; Wen, L. Tuning the autophagy-inducing activity of lanthanide-based nanocrystals through specific surface-coating peptides. *Nat. Mater.* **2012**, *11*, 817–826.
- (25) Zhu, X.; Li, J.; Qiu, X.; Liu, Y.; Feng, W.; Li, F. Upconversion nanocomposite for programming combination cancer therapy by precise control of microscopic temperature. *Nat. Commun.* **2018**, *9*, 2176.
- (26) Bettinelli, M.; Carlos, L.; Liu, X. Lanthanide-doped upconversion nanoparticles. *Phys. Today* **2015**, *68*, 38–44.
- (27) Yang, Z.; Loh, K. Y.; Chu, Y.-T.; Feng, R.; Satyavolu, N. S. R.; Xiong, M.; Nakamata Huynh, S. M.; Hwang, K.; Li, L.; Xing, H.; Zhang, X.; Chemla, Y. R.; Gruebele, M.; Lu, Y. Optical control of metal ion probes in cells and zebrafish using highly selective DNAzymes conjugated to upconversion nanoparticles. *J. Am. Chem. Soc.* **2018**, *140*, 17656–17665.
- (28) Song, G.; Hao, J.; Liang, C.; Liu, T.; Gao, M.; Cheng, L.; Hu, J.; Liu, Z. Degradable molybdenum oxide nanosheets with rapid clearance and efficient tumor homing capabilities as a therapeutic nanoplatform. *Angew. Chem., Int. Ed.* **2016**, *55*, 2122–2126.
- (29) Roy, S.; Leidal, A. M.; Ye, J.; Ronen, S. M.; Debnath, J. Autophagy-dependent shuttling of TBC1D5 controls plasma membrane translocation of GLUT1 and glucose uptake. *Mol. Cell* **2017**, *67*, 84–95.
- (30) Allen, A. E.; Locasale, J. W. Glucose metabolism in cancer: the saga of pyruvate kinase continues. *Cancer Cell* **2018**, *33*, 337–339.
- (31) Birsoy, K.; Wang, T.; Chen, W. W.; Freinkman, E.; Abu-Remaileh, M.; Sabatini, D. M. An essential role of the mitochondrial electron transport chain in cell proliferation is to enable aspartate synthesis. *Cell* **2015**, *162*, 540–551.
- (32) Sullivan, B.; Gui, D. Y.; Hosios, A. M.; Bush, L. N.; Freinkman, E.; Vander Heiden, M. G. Supporting aspartate biosynthesis is an essential function of respiration in proliferating cells. *Cell* **2015**, *162*, 552–563.